The power spectrum and correlation of flow noise for an axisymmetric body in water*

Li Xue-Gang(黎雪刚)†, Yang Kun-De(杨坤德), and Wang Yong(汪 勇)

College of Marine, Northwestern Polytechnical University, Xi'an 710072*, China*

(Received 29 October 2010; revised manuscript received 1 December 2010)

Understanding the physical features of the flow noise for an axisymmetric body is important for improving the performance of a sonar mounted on an underwater platform. Analytical calculation and numerical analysis of the physical features of the flow noise for an axisymmetric body are presented and a simulation scheme for the noise correlation on the hydrophones is given. It is shown that the numerical values of the flow noise coincide well with the analytical values. The main physical features of flow noise are obtained. The flow noises of two different models are compared and a model with a rather optimal fore-body shape is given. The flow noise in horizontal symmetry profile of the axisymmetric body is non-uniform, but it is omni-directional and has little difference in the cross section of the body. The loss of noise diffraction has a great effect on the flow noise from boundary layer transition. Meanwhile, based on the simulation, the noise power level increases with velocity to approximately the fifth power at high frequencies, which is consistent with the experiment data reported in the literature. Furthermore, the flow noise received by the acoustic array has lower correlation at a designed central frequency, which is important for sonar system design.

Keywords: flow noise, correlation analysis, power spectrum

PACS: 43.30.Nb, 43.30.Lz, 43.28.Ra **DOI:** 10.1088/1674-1056/20/6/064302

1. Introduction

Various noise sources are known to affect the performance of the sonar mounted on an underwater platform, such as autonomous underwater vehicle (AUV) and underwater unmanned vehicle (UUV). These noise sources include hydrodynamic noise, ambient noise, propeller noise and mechanical noise. Flow noise as a main part of the hydrodynamic noise dominates all other sources combined. It covers the radiated noise of a target in far field and limits the performance of self-sonar. If the self-noise level of the underwater body can reduce 10 dB, the detection range of the sonar will increase 2 to 3 times under the same condition. Thus it is necessary to study the physics of flow noise and find the way to reduce or even suppress it.

In the past few years, several methods were used to calculate the flow field and noise field. Mak and Wu,[1] Mak and Au,[2] and Han and Mak[3] predicted the flow noise from spoiler in ducts. Lighthill[4,5] presented the acoustic analogy theory, by which the physical model of the hydrodynamic noise can be simplified. Haddle and Skudrzk[6] presented the physics of the flow noise and measured the radiated noise from a rising buoyant unit. Based on the Lighthill theory, Lauchle[7,8] derived the model of the noise generated by axisymmetric turbulent boundary layer flow and made an experimental effort to characterize the broadband flow-induced self-noise on a spherically shaped acoustic velocity sensor operating in water. Due to the complex reverberation[9] and dispersive propagation[10] in the shallow water, the measurements of flow noise were still restricted in the laboratory.[11]

All the above methods were used mainly to calculate the flow field and the power spectrum of the flow noise. In this paper, the radiated noise from the transition of an axisymmetric body is calculated. Meanwhile a calculation process for the noise correlation of the hydrophones mounted on the axisymmetric body is presented. With the renormalization group (RNG) k–ε two equation turbulent models, the three-dimensional viscous flow fields are calculated by two models. Using the solution of the viscous field, the Ffowcs Williams and Hawkings (FW-H)[12] acoustic model is added to simulate the unsteady flow field and noise field. Then the physical characteristics of

*Project supported by the National Natural Science Foundational of China (Grant No. 10774119), the Program for New Century Excellent Talents in University, China (Grant No. NCET-08-0455), the Natural Science Foundation of Shaanxi Province of China (Grant No. SJ08F07), and the Foundation of National Laboratory of Acoustic and the Foundation for Fundamental Research of Northwestern Polytechnic University, China (Grant No. 2007004).

†Corresponding author. E-mail: xuegang608@126.com

© 2011 Chinese Physical Society and IOP Publishing Ltd

the flow noise are analysed. The sound power spectra obtained from the two models are compared and a better model shape from the viewpoint of noise spectrum is given. Furthermore, the correlations of noise field received by the acoustic array are calculated and analysed.

2. Analytical calculation method

2.1. Flow noise from transition region

The boundary layer of an axisymmetric body is shown in Fig. 1. The source of flow noise under consideration is the transition region and the turbulent boundary layer on the axisymmetric body. Lauchle[7] has shown that the noise measured in the laminar region (including the stagnation point) corresponds closely to that measured in the transition region, provided that the acoustic losses due to diffraction are taken into account. Experimental results[13] show that when the frequency of the flow noise is less than 40 kHz, the flow noise received at the stagnation point of the axisymmetric body is mainly from the transition region.

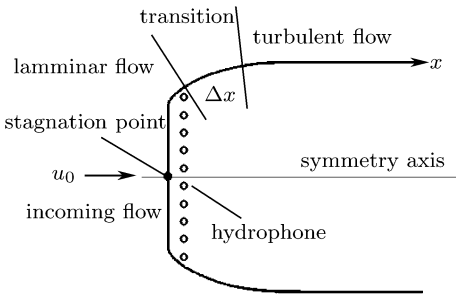


Fig. 1. Boundary layer of the axisymmetric body.

Based on the Liepmann's theory, the sound power spectrum $G(r,f)$ received at the stagnation point of the axisymmetric body can be written as[14]

$$G(r,f)=\frac{W\rho^2u_0u_c\Delta\delta^{*2}(k_c\Delta x)^2}{8\pi^2r^2[1+(k_c\Delta x)^2]\left(\dfrac{t_iu_c}{\Delta x}\right)^2}F(k_c\Delta x), \quad (1)$$

where

$$F(k_c\Delta x)=(k_c\Delta x)^2\times\int_0^1\int_{-z}^{1-z}\frac{zN^*\gamma\cos(k_c\Delta xy)\,\mathrm{e}^{-\alpha^*\Delta x|y|}}{4N^{*2}\left(\dfrac{u_0}{u_c}\right)^2+(k_c\Delta x)^2}\mathrm{d}y\mathrm{d}z \quad (2)$$

with

$$\alpha^*=(1+83.35z^8)/\Delta x, \quad (3)$$

$$\gamma(z)=1-\mathrm{e}^{-(1+3.4z)z^2}, \quad (4)$$

$$N(z)=2.38\frac{u_0}{\Delta x}\sqrt{(1-\gamma)\mathrm{In}\frac{1}{1-\gamma}}, \quad (5)$$

and

$$N^*=N\cdot\Delta x/u_c; \quad (6)$$

W is the perimeter of the axisymmetric body in the transition region; ρ is the fluid density; u_0 is the free-stream flow velocity; $u_c=0.8u_0$ and $t_iu_c/\Delta x=0.45$ represent parameters fitted to experiment data; $\Delta\delta^*$ and Δx denote the displacement thickness and the length of the transition region, respectively; r is the distance from the transition region to the stagnation point; $k_c=\omega/u_c$ is the wave number. The distributions for the intermittency factor and burst frequency given in Eqs. (4) and (5), respectively, are taken from Josserand's experimental data.[14]

Equation (2) has been integrated numerically by Simpson's rule. A typical result of this computation is presented in Fig. 2. It is seen that the magnitude of the high-frequency portion of the spectrum depends on the value of $k_c\Delta x$. At very low values of $k_c\Delta x$, the spectral levels rise at 12 dB/oct. For $k_c\Delta x\gg1$, the spectrum levels roll off at 6 dB/oct.

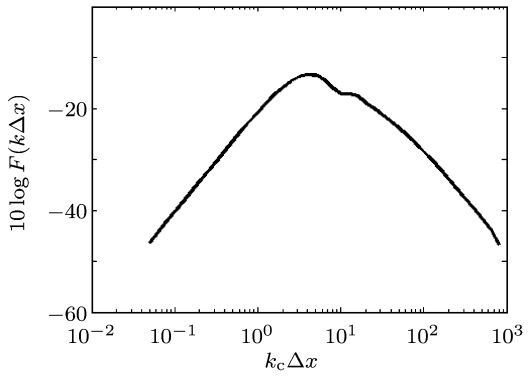


Fig. 2. Power spectrum density function of Eq. (2).

2.2. Effects of acoustic diffraction

For the receiving points located in the laminar flow regions, the noise recorded originates from elsewhere in the flow. This can be verified through the consideration of the acoustic loss as a function of frequency, due to acoustic diffraction. The signal recorded at the stagnation point would show the greatest loss due to diffraction effect. It is assumed that the transition region is the dominant source of sound,

which can be considered as a ring of uncorrelated point sources. When the wavelength of the sound wave is much longer than the diameter of the axisymmetric body, the loss of noise diffraction can be ignored. However, when the frequency of the sound wave is high, the loss of noise diffraction along the head of the axisymmetric body would become larger as the frequency increases.

Arakeri[13] has derived the following expression for the diffraction loss around a rigid contour of an elliptic shape:

$$\Delta S_{\mathrm{d}} = \begin{cases} 0, & f \le f_{\mathrm{c}}, \\ \psi(f) - \psi(f_{\mathrm{c}}), & f > f_{\mathrm{c}}, \end{cases} \tag{7}$$

with

$$\psi(f) = 20\log\left\{\frac{\left(\frac{A}{B}\right)^{1/2}\exp\left[-\cos\left(\frac{\pi}{6}\right)\left(\frac{k}{A}\right)^{1/3}\left(\frac{9\pi B}{4}\right)^{2/3}\frac{F(\kappa)}{2}\right]}{4\sqrt{\frac{D}{2}x_1}q_0\mathrm{A_i}(q_0)}\right\}, \tag{8}$$

where

$$F(\kappa) = \int_0^{\pi/2}\left(1-\kappa^2\sin^2\varphi\right)^{-1/2}\mathrm{d}\varphi, \tag{9}$$

$$\kappa^2 = \frac{A^2-B^2}{A^2}, \tag{10}$$

A and B are the major and minor axes of the ellipse respectively, D is the biggest diameter of the axisymmetric body; $f_{\mathrm{c}} = 2c/D$ is the critical frequency; k is the wave number; $\mathrm{A_i}$ is the Airy function of the first kind; q_0 is the first zero point of $\mathrm{A_i'}(q)$ where the prime denotes the derivative with respect to argument.

When the peak of the axisymmetric body is flat, a modified coefficient ΔU_{d} should be added to Eq. (8). The following expression for ΔU_{d} is used:

$$\Delta U_{\mathrm{d}} = -20\log\left[\left(\frac{B^2}{A}\right)^{-1/3}2^{5/6}3^{1/3}\pi^{-1/2}k^{1/6} \times \left(\frac{D}{2}-B\right)^{1/2}\mathrm{A_i}(q_0)\right]. \tag{11}$$

3. Numerical simulation method

The analytical method described in Section 2 can only calculate the power spectrum of the flow noise. It cannot be used to calculate the noise correlations of the hydrophones mounted on the axisymmetric body. The noise correlations of the hydrophones can be calculated by the following numerical method.

3.1. Flow field equations

According to the laws of mass conservation and momentum conservation, the Navier–Stokes (NS)[15] equations of viscous fluid can be written as

$$\frac{\partial u_i}{\partial x_i} = 0, \tag{12}$$

$$\frac{\partial u_i}{\partial t} + u_j\frac{\partial u_i}{\partial x_j} = f_i - \frac{1}{\rho}\frac{\partial p}{\partial x_i} + \frac{\partial}{\partial x_j}\left(v\frac{\partial u_i}{\partial x_j} - \overline{u_i'u_j'}\right), \tag{13}$$

where v is the kinematical viscosity coefficient, p is the average pressure, (x_i, x_j) denotes the particle coordinates each of which is a function of t, u_i, and u_i' are the average velocity and the velocity fluctuation of the fluid, respectively.

The Reynolds stress $\overline{u_i'u_j'}$ can be determined by the following turbulence model:

$$-\overline{u_i'u_j'} = v_{\mathrm{t}}\left(\frac{\partial u_i}{\partial x_j} + \frac{\partial u_j}{\partial x_i}\right) - \frac{2}{3}k\delta_{ij}, \tag{14}$$

$$v_{\mathrm{t}} = C_\mu\frac{k^2}{\varepsilon}, \tag{15}$$

where δ_{ij} is the Kronecker symbol, v_{t} is the turbulent viscosity, k and ε denote the turbulent energy and the dissipation rate respectively, and C_μ is a constant.

The RNG k–ε two-equation turbulent model[16] used in this paper is given by

$$\frac{\partial}{\partial t}(\rho k) + \frac{\partial}{\partial x_j}(\rho k u_j) = \frac{\partial}{\partial x_j}\left[\left(\mu + \frac{\mu_t}{\sigma_k}\right)\frac{\partial k}{\partial x_j}\right] + G_k - \rho\varepsilon, \tag{16}$$

$$\frac{\partial}{\partial t}(\rho\varepsilon) + \frac{\partial}{\partial x_j}(\rho\varepsilon u_j) = \frac{\partial}{\partial x_j}\left[\left(\mu + \frac{\mu_t}{\sigma_\varepsilon}\right)\frac{\partial \varepsilon}{\partial x_j}\right] + C_{1\varepsilon}\frac{\varepsilon}{k}G_k - C_{2\varepsilon}\rho\frac{\varepsilon^2}{k}, \tag{17}$$

where C_μ, σ_k, σ_ε, $\sigma_{1\varepsilon}$, and $\sigma_{2\varepsilon}$ are constants of the model.

The RNG theory provides an analytical formula for turbulent Prandtl number but not a constant. This improvement achieves good results in the simulation accuracy and the range of application. The flow field can be obtained by solving the NS equations and RNG

k–ε two-equation turbulent model with the FLUENT software.[16]

3.2. Acoustic field equations

Based on the flow field model given in Subsection 3.1, the generalized Lighthill equation[4,5] in acoustic analogy theory is used to calculate the noise field. Its density wave equation is in the form of

$$\frac{\partial^2 \rho'}{\partial t^2} - a_0^2 \nabla^2 \rho' = \frac{\partial^2 T_{ij}}{\partial x_i \partial x_j}, \tag{18}$$

$$T_{ij} = \rho u_i u_j - \sigma_{ij} + \delta_{ij}[(p - p_0) - a_0^2(p - p_0)], \tag{19}$$

where T_{ij} is the Lighthill stress tensor, a_0 is the sound speed in the isentropic fluid, ρ and ρ_0 denote the fluid densities with disturbance and without disturbance, respectively. ρ' equals $\rho - \rho_0$, which is the change in the density caused by fluid disturbance.

Based on the Lighthill's acoustic analogy theory, Ffowcs Williams and Hawkins[12] obtained the FWH equation by using the generalized function, which is used in this paper to simulate the flow noise.

4. Calculation process for flow noise

The calculation process of the flow noise for an axisymmetric body is shown in Fig. 3. When the geometrical shape of an axisymmetric model is given,

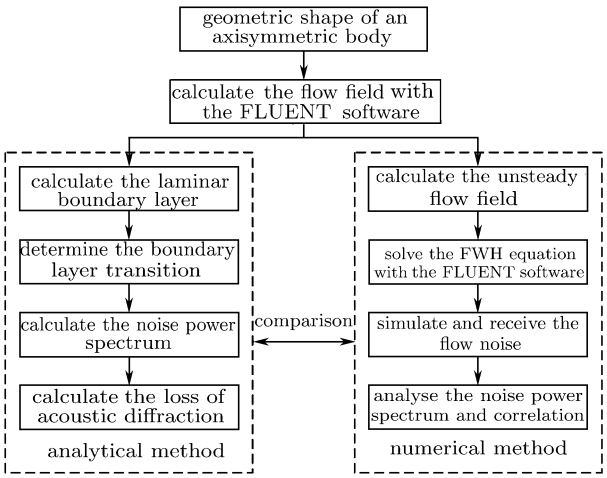


Fig. 3. Calculation process of the flow noise.

the flow noise of the model can be calculated by the analytical method and numerical method. For the analytical method, the laminar boundary layer can be solved by the Thwaits's method.[17] The boundary layer transition is determined using the Granville curve and then the power spectrum of the flow noise can be calculated. For the numerical method, the flow field can be calculated by solving the NS equations with the FLUENT software. The FWH acoustic model is added to simulate the noise field. Finally, the results of the two methods are compared and the power spectrum and correlation of the flow noise are analysed.

5. Results and discussion

5.1. Analytical results

In this section the flow noise calculation method is introduced for the two models with different forebody shapes. The unstable point and transition point are estimated and then the length of the boundary layer transition is computed. Finally, the self-noises of the models are calculated. As shown in Fig. 4(a), the diameter of the model A is larger than that of the model B at the head of the axisymmetric body. In other parts, the geometries of the two models are both the same. The pressure field and the velocity field can be calculated by the FLUENT software.[16] The fluid velocity is assumed to be 42 knots (about 21.6 m/s). The pressure coefficients of the two models along the upper meridian line are shown in Fig. 4(b). The minimum pressure points are 22 mm and 83 mm away from the peak for the model A and model B, respectively.

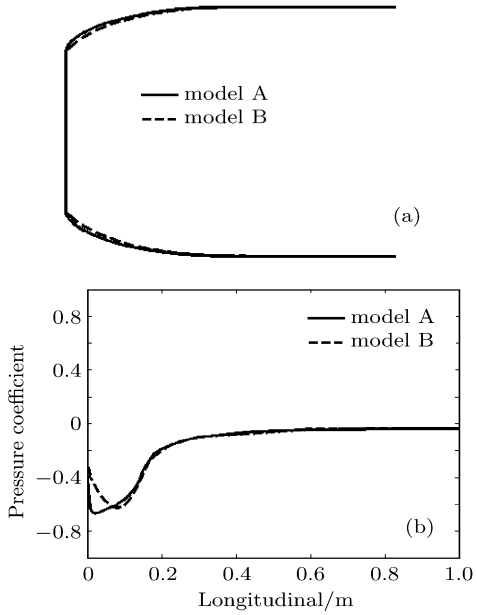


Fig. 4. Two axisymmetric models with (a) different forebody shapes and (b) different pressure coefficients.

In order to determine the boundary layer transition Δx in Eq. (2), the following approach is used.

The length of the boundary layer transition Δx can be calculated by the following equation:

$$\Delta x = x_{\rm tr} - x_{\rm cr}, \tag{20}$$

where $x_{\rm cr}$ and $x_{\rm tr}$ are the unstable point and the transition point, respectively.

It is difficult to determine the unstable point $x_{\rm cr}$. We replace $x_{\rm cr}$ with the minimum pressure point in Fig. 4(b). The transition point $x_{\rm tr}$ can be obtained by the Granville's method.[17] As shown in Fig. 4, the solid curve can be generated by the following equation:

$$Re_{\theta{\rm tr}} - Re_{\theta{\rm cr}} = \sum_{n=0}^{4} D_n \lambda_\theta^n, \tag{21}$$

where $D_0 = 820.571$, $D_1 = 28273.8$, $D_2 = 707219$, $D_3 = 5167690$, and $D_4 = 22302300$.

The dotted curve is drawn by $Re_\theta(x)$–$Re_\theta(x_{\rm cr})$ and $\lambda_\theta(x)$. $Re_\theta(x)$ and $Re_\theta(x_{\rm cr})$ are Reynolds numbers with taking the momentum thickness as the characteristic length and $\lambda_\theta(x)$ is the average pressure gradient. These parameters can be calculated by the method in Ref. [17]. The transition point $x_{\rm tr}$ of the model corresponds to the intersection of the two curves in Fig. 5. The lengths of the boundary layer transition are 62 mm and 47 mm for the model A and model B, respectively.

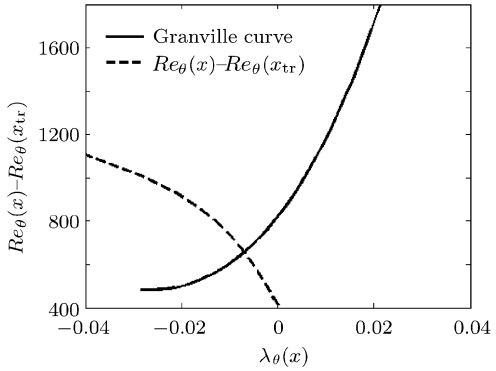


Fig. 5. The Granville method to determine the transition point.

Based on the method described above, the radiated noise from transition region can be calculated. The sound power spectra of the two models are shown in Fig. 6. The noise power level of the model A is 1 dB to 6 dB higher than that of the model B in a frequency range from 100 Hz to 40 kHz. The intersection of the curves corresponds to the critical frequency $f_{\rm c}$. When the frequency f is smaller than $f_{\rm c}$, the loss of noise diffraction is not considered. When the frequency f is higher than $f_{\rm c}$, the loss of noise diffraction is calculated by Eqs. (7)–(11). It is shown that the effects of acoustic diffraction cannot be ignored at high frequencies.

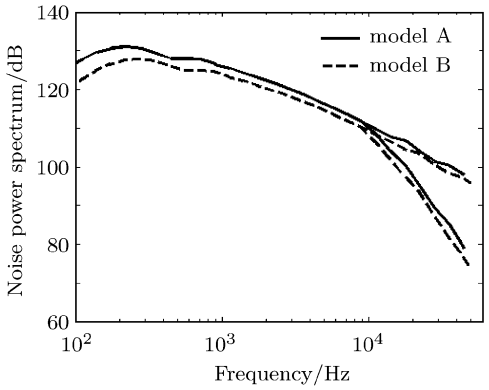


Fig. 6. Power spectra of the flow noise for the two models.

5.2. Numerical results and discussion

Through the following two steps, the flow field and the noise field are simulated. In the first step, the unsteady flow field is computed by solving the NS equations. In the second step, the K-FWH integration approach is used to calculate the noise field. Three-dimensional, discrete, implicit and unsteady solvers are set in the FLUENT software. In order to obtain high frequencies of the flow noise, the time step is set to be 0.01 ms. The reference pressure is 1 μPa. The sound speed in the medium is assumed to be 1500 m/s. The surface meshing of the model is shown in Fig. 7. The Reynolds number Re is 5.4328×10^7, with taking the length of the model as the characteristic length.

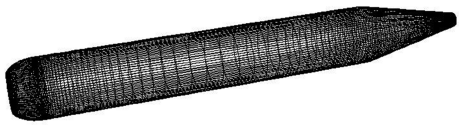


Fig. 7. Surface meshing of the model.

The sound power spectra of the two models are shown in Fig. 8. The solid lines and dotted lines in Figs. 8(a) and 8(b) represent the analytical values and numerical values, respectively. It can be seen that the analytical values of the flow noise are compared well with the numerical values. The solid line and the dotted line in Fig. 8(c) are fitted by the numerical values in Fig. 8(a) and Fig. 8(b) respectively. In Fig. 8(d), $G_{\rm A}$ and $G_{\rm B}$ are the fitting values in Fig. 8(c), corresponding to model A and model B, respectively. It is seen that the sound power spectrum in the peak of model A is higher than that of model B in majority frequencies, which indicates that the fore-body shape of model B is better than that of the model A.

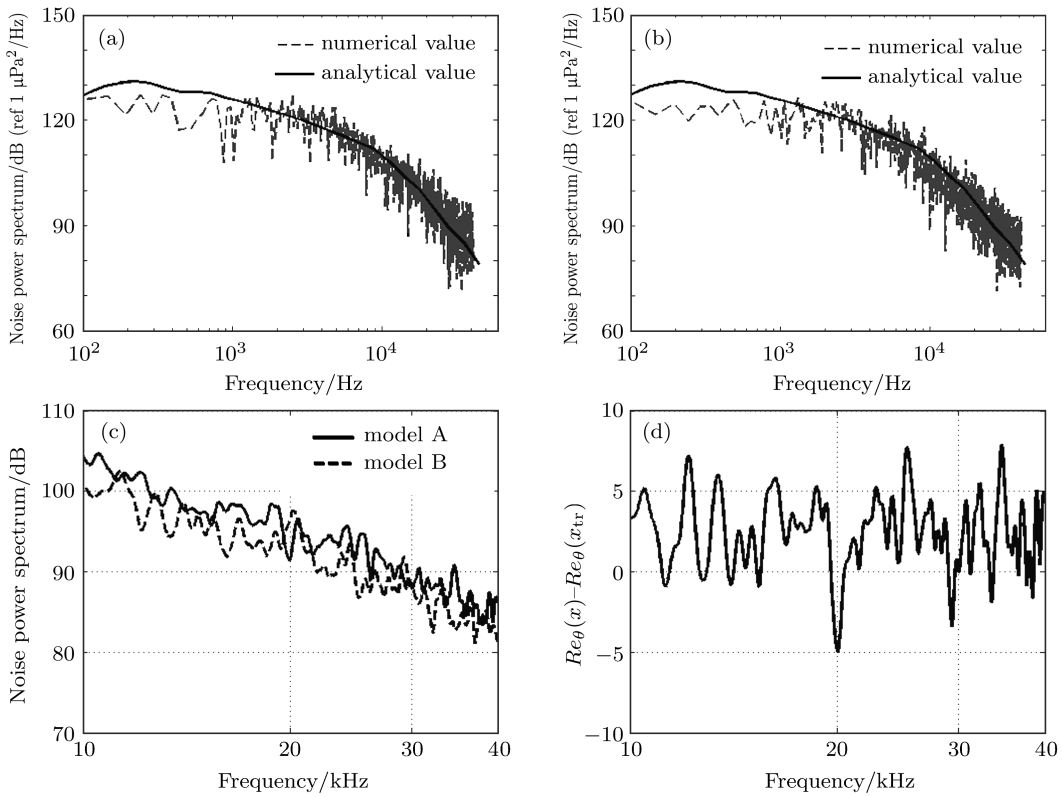


Fig. 8. Noise power spectra at the stagnation point of the two bodies: (a) flow noise of the model A, (b) flow noise of the model B, (c) fitting flow noise at 10 kHz ∼ 40 kHz for model A and model B, and (d) difference values of the two models.

The sound power level of the flow noise in the horizontal symmetry profile of the axisymmetric body is shown in Fig. 9(a). It is shown that the radiated noise in the horizontal symmetry profile is non-uniform. The flow noise around the model is strong and it becomes weaker in the far-field. Radiated noise in the cross section is shown in Fig. 9(b). Twelve receiving points are distributed uniformly in a circle. The centre of the circle is on the symmetry axis and it is 1.4 m away from the peak of the body. The radius of the circle is 1.0 m. The power spectrum levels at the twelve receiving points are reduced 60 dB to show the spatial distribution of the radiated noise clearly. It is seen that the sound power level of the model A is 1 dB to 2 dB higher than that of model B at 30 kHz. The radiated noise is omni-directional and has few differences in the cross section.

The noise power levels of the flow noise along the symmetry axis of the two models are shown in Fig. 10. It is seen that the average power level of the model A is 1 dB to 4 dB higher than that of the model B in the frequency range from 25 kHz to 35 kHz. The noise power levels in the peak of both the models are small, which provides us with an important theoretical support for laying acoustic arrays.

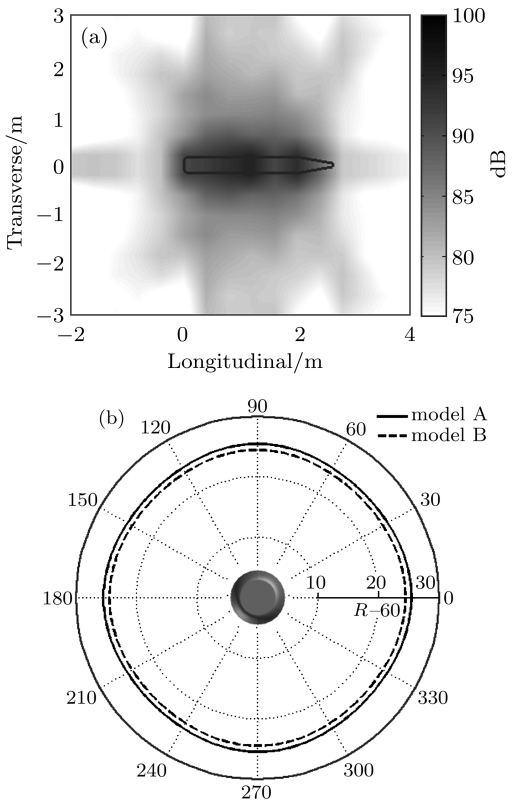


Fig. 9. Spatial distributions of the radiated noises in the horizontal profile (a) and the cross section (b).

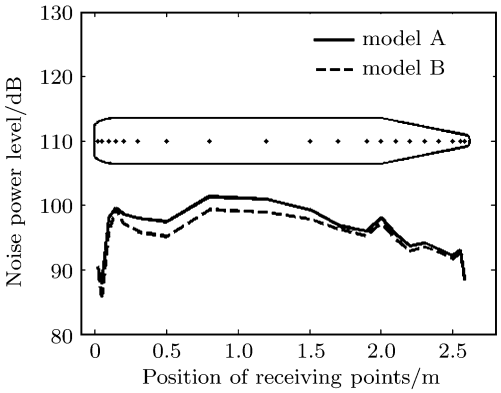


Fig. 10. Noise power levels of the two models with different fore-body shapes.

Figure 8 shows the noises received at the stagnation point for three typical free-stream velocities. It is seen from Fig. 8(b) that the noise power levels increase with velocity to approximately the fifth power at high frequencies, which is consistent with the Lauchle's experimental data.[18] Based on the Lighhill equation, Lauchle[18] derived the relationship between the noise power and free-stream velocity by the method of dimensional analysis. The relationship is given by

$$G(r, f) \propto u_0^5. \tag{22}$$

As shown in Fig. 11, a line array with 10 hydrophones was mounted in the head of the axisymmetric body and it is 20 mm away from the peak of the body. The spacing between the adjacent hydrophones is 25 mm on the assumption that the designed central frequency is 30 kHz based on the array configuration method of half-wavelength. The flow noise calculated by the FLUENT software is the broadband noise, whose frequency is in a range from 0 kHz to 50 kHz. Four band-pass filters are used to filter the flow noise. The frequency bandwidths of the four filters are 9.5 kHz–10.5 kHz, 19 kHz–21 kHz, 27.5 kHz–32.5 kHz, and 35 kHz–40 kHz. The noise correlations of the hydrophones are shown in Fig. 12. The colour value of each square denotes the correlation coefficient of the two hydrophones on the lower left corner of the square. It can be seen that the correlation on the hydrophones has no obvious feature and the correlation at low frequencies is stronger than that at high frequencies. Because the frequencies are lower than the designed central frequency.

In Fig. 13, f_c is the central frequency of the filter and the bandwidths of both filters are 5 kHz. It is seen that the correlation coefficient depends on the hydrophone spacing and frequency. The flow noise received by the line array has lower correlation at the designed central frequency, which is important for sonar system design.

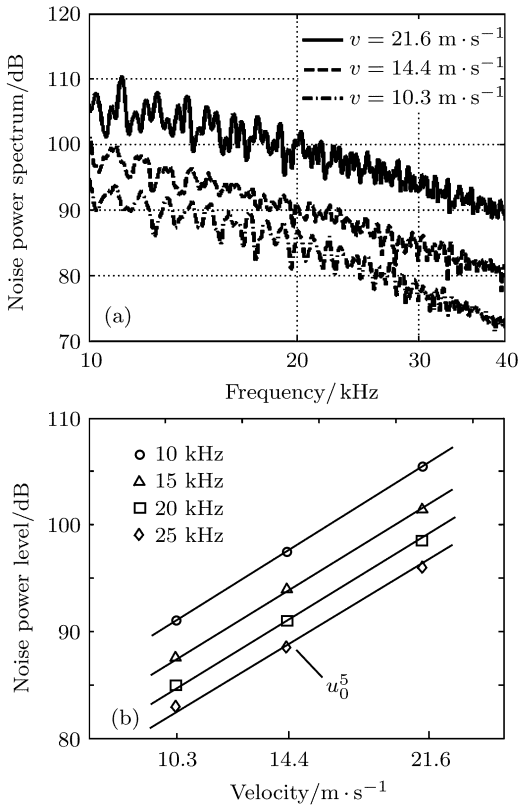
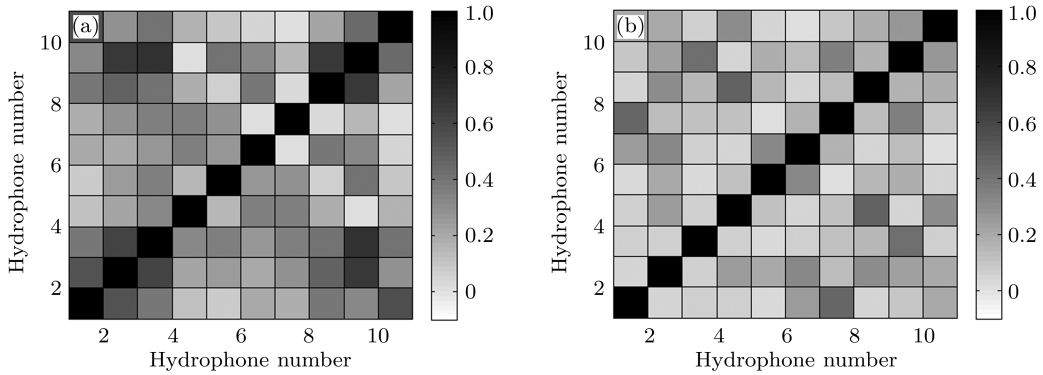


Fig. 11. Noise spectra recorded at the stagnation point for three different free stream flow velocities (a) and for three different frequencies (b).



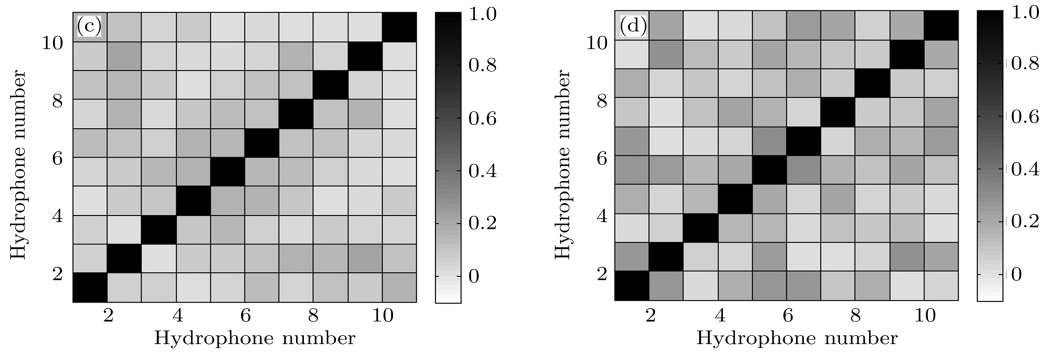


Fig. 12. Correlations between hydrophones in frequency ranges from (a) 9.5 kHz to 10.5 kHz, (b) 19 kHz to 21 kHz, (c) 27.5 kHz to 32.5 kHz, (d) 35 kHz to 45 kHz.

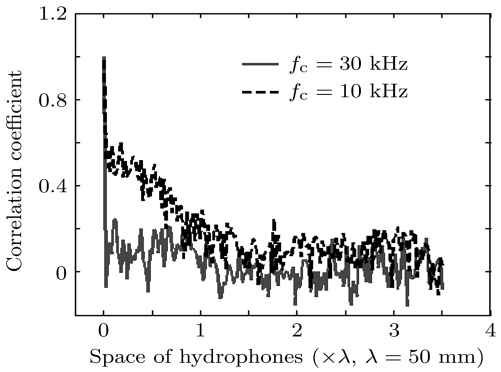


Fig. 13. Dependence of correlation coefficient on hydrophone spacing for two different frequencies.

6. Conclusions

The physical features of the flow noise for an axisymmetric body are important for improving the performance of a sonar mounted on an underwater platform. Based on the numerical calculation of the flow noise for an axisymmetric body, a calculation process for the noise correlation of hydrophones mounted on the axisymmetric body is presented. The flow noises for two axisymmetric models are studied by the analytical calculation method and numerical simulation method separately. The following results are obtained. (i) The numerical values of the flow noise for the two models coincide well with the analytical values. (ii) The flow noise received by the line array has a lower correlation at central frequency, which is important for sonar system design. (iii) By comparing the flow noises of the two models, a rather optimal fore-body shape of model is given, which could be used to design an axisymmetric body for minimum self-noise. (iv) The noise power level depends on the velocity greatly and increases with velocity to approximately the fifth power at high frequencies, which is consistent with the experiment data. (v) The loss of noise diffraction has a great effect on the flow noise from boundary layer transition region, especially at high frequencies. (vi) The radiated noise in horizontal symmetry profile of the axisymmetric body is non-uniform, but it is omni-directional and has little difference in the cross section.

In addition, the experiment designed to confirm the physical features of flow noise, such as the power spectrum and correlations, will be the future work. Meanwhile, it is also valuable to study how to make full use of the noise correlation in the acoustic array signal processing.

References

[1] Mak C M and Wu J 2009 *J. Acoust. Soc. Am.* **125** 3756
[2] Mak C M and Au W M 2009 *Appl. Acoust.* **70** 11
[3] Han N and Mak C M 2008 *Appl. Acoust.* **69** 566
[4] Lighthill M J 1952 *Proc. Roy. Soc. London* Ser A **211** 564
[5] Lighthill M J 1954 *Proc. Roy. Soc. London* Ser A **222** 1
[6] Haddle G P and Skudrzk E J 1969 *J. Acoust. Soc. Am.* **46** 130
[7] Lauchle G C 1980 *J. Acoust. Soc. Am.* **67** 158
[8] Lauchle G C 1997 *J. Acoust. Soc. Am.* **101** 3053
[9] Hui J, Wang Z J, Hui J Y and He W X 2009 *Acta Phys. Sin.* **58** 5491 (in Chinese)
[10] Tang L G, Xu X M and Liu S X 2008 *Acta Phys. Sin.* **57** 4251 (in Chinese)
[11] Lei B, Yang K D and Ma Y L 2010 *Chin. Phys.* B **19** 054301
[12] Ffowcs Williams J E and Hawking D L 1969 *Phil. Trans. Roy. Soc.* **264A** 321
[13] Arakeri V H 1991 *J. Sound. Vib.* **146** 449
[14] Lauchle G C 1981 *J. Acoustic. Soc. Am.* **69** 665
[15] Zhang Z S and Cui G X 1999 *Fluid Mechanics* (Beijing: Tsinghua University Press) p. 251 (in Chinese)
[16] Li J L and Li C X 2009 *Master Fluent* 6.3 *for Flow Field Analyses* (Beijing: Chemical Industry Press) p. 150 (in Chinese)
[17] Huang J Q and Zhang Y W 1989 *Hydromechanics of an Axisymmetric Body.* (Xi'an: Northwestern Polytechnical University Press) p. 112 (in Chinese)
[18] Lauchle G C 1977 *J. Acoust. Soc. Am.* **61** 694